Editors' Suggestion

Coupling of a Nuclear Transition to a Surface Acoustic Wave

Albert Nazeeri,[1] Chiara Brandenstein,[1] Chengjie Jia,[1] Lorenzo Magrini,[1,*] and Giorgio Gratta[1,2]
[1]Department of Physics, Stanford University, Stanford, California 94305, USA
[2]Hansen Experimental Physics Lab, Stanford University, Stanford, California 94305, USA

(Received 8 September 2025; revised 5 February 2026; accepted 16 March 2026; published 5 May 2026)

Mechanical modulation of recoilless nuclear transitions allows the dynamic control of γ-ray emission and absorption. Accessing modulation frequencies well above the nuclear linewidth enables coherent manipulation of the nuclear response. Here we demonstrate high-frequency control via efficient coupling of a film of enriched ^{57}Fe to a 97.9 MHz surface acoustic wave, nearly 2 orders of magnitude higher than the nuclear linewidth. The mechanical drive produces a comb of absorption sidebands in the Mössbauer spectrum, reflecting the periodic time modulation of the nuclear transitions. This constitutes the highest frequency mechanically driven Mössbauer resonance to date. Our solid-state, monolithic platform establishes a new interface between nuclear transitions and high-frequency acoustics, with applications in γ-ray quantum optics and precision nuclear spectroscopy.

DOI: 10.1103/tc97-98f7

Introduction—When low-energy nuclear γ transitions occur in certain solids, the recoil can be coherently absorbed by the entire lattice. This results in a recoil-free transition that is characterized by extremely narrow spectral lines and is known as the Mössbauer effect [1]. Discovered in 1958, the Mössbauer effect was soon employed in a landmark experiment to measure the gravitational redshift, one of the predictions of general relativity [2]. Today, Mössbauer spectroscopy is a useful tool in chemistry and materials science; shifts of the extremely narrow resonances are sensitive local probes to the electric, magnetic, and structural environments of Mössbauer active atoms. [3]. Beyond precision spectroscopy, the Mössbauer effect is a fundamental tool in nuclear and x-ray quantum optics [4–7]. Coherent control of a nuclear ensemble, achieved through external magnetic fields [8] or mechanical modulation [9–11], has enabled demonstrations such as waveform shaping of recoilless γ-ray photons [12] and spectral narrowing of synchrotron pulses [13]. Here, we demonstrate the coupling of enriched ^{57}Fe nuclei to a traveling surface acoustic wave (SAW) at 97.9 MHz in a monolithic device. This approach offers three fundamental advantages over bulk piezodriven films. First, it enables modulation of nuclear resonances at frequencies well above the nuclear linewidth, extending the accessible modulation bandwidth beyond what has been achieved with conventional piezo-driven schemes [10–13]. Second, the fabrication of surface acoustic wave devices is well controlled and scalable, with considerable flexibility in the design. Third, SAWs constitute a mature solid-state platform well understood in the quantum regime [14–16] and compatible with a wide variety of quantum systems [17–19].

We observe Floquet sidebands of the nuclear transitions, with intensities following the characteristic Bessel-function dependence on the modulation strength. To our knowledge, this represents the highest-frequency phonon-driven modulation of Mössbauer resonances reported to date, and the first realized in a monolithic device, establishing a new method for high-bandwidth, time-resolved mechanical control of nuclear resonances.

Experiment—To enable high-frequency mechanical modulation of nuclear resonances, an ^{57}Fe film is deposited on a ST-cut [20] quartz substrate, and the film is driven by a 97.9 MHz surface acoustic wave. This modulated Mössbauer absorber is placed in a conventional transmission spectrometer [21] [Fig. 1(a)]. The Mössbauer absorber is fabricated by thermally evaporating iron enriched to 96% in the isotope ^{57}Fe, forming a 200-nm-thick film. The deposition is obtained in a dedicated setup at a pressure of 9.5×10^{-10} Torr and a deposition rate of 6.1 nm/h. This fully monolithic implementation, using surface acoustic waves to avoid intermediate, lossy adhesive layers, concentrates the mechanical energy near the surface, resulting in larger Doppler velocities per unit power compared to bulk acoustic transducers.

With no SAW excitation, the absorption spectrum is dominated by hyperfine Zeeman interactions in the ^{57}Fe film which splits the nuclear ground (excited) state into 2 (4) hyperfine states of angular momentum $m_j = \pm 1/2$ ($m_j = \pm 1/2, \pm 3/2$) [purple lines in Figs. 1(b) and 1(c)]. The selection rule $\Delta m_j = 0, \pm 1$ then leads to 6 different allowed transitions [3], spaced by 101 neV (corresponding to 24.4 MHz, or a Doppler velocity of 2.1 mm/s),

*Contact author: magrini@stanford.edu

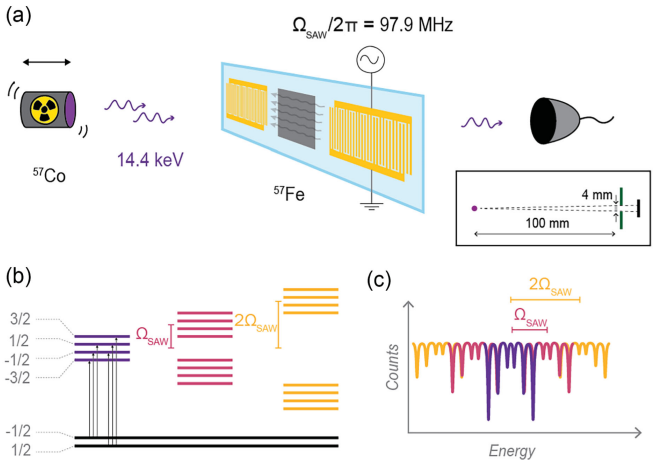

FIG. 1. (a) Schematic view of the experiment. A (0.9×4.0) mm^2 film of ^{57}Fe is deposited between two SAW couplers on a quartz substrate and characterized in a Mössbauer spectrometer. The inset shows the setup to scale, with the SAW device and ^{57}Fe absorbing film (gray) placed at a distance of 10 cm from the ^{57}Co source (purple). A tungsten collimator (green) blocks all noninteracting photons from reaching the detector (black). (b) Nuclear level scheme, showing the unmodulated hyperfine transitions (purple) and the first-order (magenta) and second-order (yellow) vibrational sidebands driven by the SAW. (c) Illustration of the expected spectrum without (purple) and with (all colors) the SAW drive on.

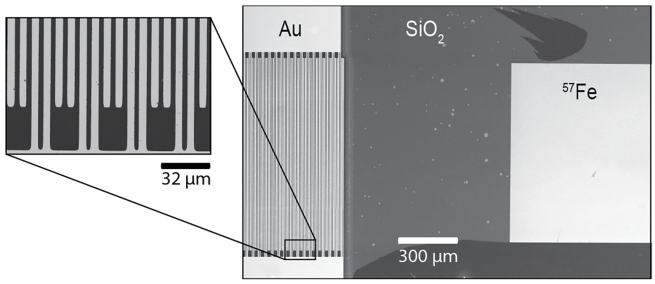

FIG. 2. Main panel: microphotograph of part of the absorber device on the quartz substrate, including sections of the ^{57}Fe film and of one of the SAW couplers. Inset: higher magnification detail of one of the SAW couplers.

schematically shown in the bottom panel of Fig. 1(b). The data shown in this Letter were taken on a device where overetching in the final step resulted into a reduction of the total amount of iron, so that the effective thickness was approximately 90 nm over a region of (0.9×4.0) mm^2 (thickness estimated by the contrast of the peaks in the absorption spectrum) [22]. SAWs are excited in the quartz by two sets of interdigitated transducers (IDTs or "couplers") deposited at opposite ends of the chip, with a pattern of double lines, spaced by a $\lambda_{SAW} = 32$ μm pitch, illustrated in Fig. 2. The pattern is designed to resonantly couple, by piezoelectric effect, $\Omega_{SAW} = 2\pi \times 97.9$ MHz SAWs propagating across the chip. The two opposite couplers allow for testing the coupling from electric signals, to acoustics, and back to electric signals. To avoid reflections off the edge of the substrate, the edges of the quartz chip are "terminated" by small pieces of kapton tape. A fraction, α, of the SAW is still coherently reflected by the impedance mismatch from the readout coupler. This reflection gives rise to a partial standing wave across the quartz chip. The resulting modulation of the SAW amplitude is included in the spectral analysis. A 1 GBq ^{57}Co source was used for the experiment, where the ^{57}Co is embedded in a rhodium matrix, resulting in a single emission line of $E_\gamma \simeq 14.4$ keV, an isomer shift with respect to α-Fe of -5 neV, and a linewidth of 7 neV (1.7 MHz), slightly broader than the natural linewidth of the nuclear state. The absorption spectrum of the ^{57}Fe film is scanned by varying the Doppler shift between the source and absorber. The highest contrast of the absorption resonances is about 3%, so that the count rate is dominated by nonresonant γ rays background (14.4 keV and Compton scattering of 122 keV). A tungsten collimator is used to increase the contrast of the resonances, resulting in a count rate of approximately 2 kHz, consistent with the internal conversion coefficient and solid angle defined by the collimator [22]. For each spectrum collected, about 10 days of data are required to sufficiently suppress Poisson fluctuations. The amplitude of the SAW generated by the coupler is given by $A = C_\perp \eta \sqrt{P_{in}}$, where P_{in} is the applied rf power, $\eta = 0.35$ is the overall electroacoustic attenuation [22], and $C_\perp$ is the out-of-plane displacement conversion constant (in units of $m/\sqrt{W}$) that depends on the mechanical properties of the substrate and the width of the IDTs. The attenuation factor η accounts for losses due to electrical reflection, device geometry, acoustic attenuation, and other nonidealities. The SAW displacement modulates the nuclear transition energy via the Doppler effect. When the SAW is driven at an angular frequency Ω_{SAW}, the nuclear levels are periodically shifted, resulting in sidebands spaced by Ω_{SAW} [Figs. 1(b) and 1(c)]. For a pure traveling surface acoustic wave, the resulting absorption spectrum is given by [11,22,23]

$$S(\Omega) = \sum_i \sum_{n=-\infty}^{\infty} \frac{s_i J_n^2(k_0 A)}{(\Omega - \Omega_i - n\Omega_{SAW})^2 + \left(\frac{\Gamma}{2}\right)^2}, \quad (1)$$

where k_0 is the photon wave number, and Ω_i and s_i are the angular frequency and relative intensity of the ith hyperfine transition, $J_n(k_0 A)$ denotes the nth-order Bessel function of the first kind, and Γ is the transmission linewidth in units of angular frequency, given by the sum of the linewidths of the source and absorber. The relative prominence of the sidebands depends on the applied SAW power, which is varied in the experiment to characterize the device. For each setting a spectrum is acquired by scanning the source velocity from $-19 < v < +19$ mm/s under constant acceleration. Within this velocity range each spectrum reveals up

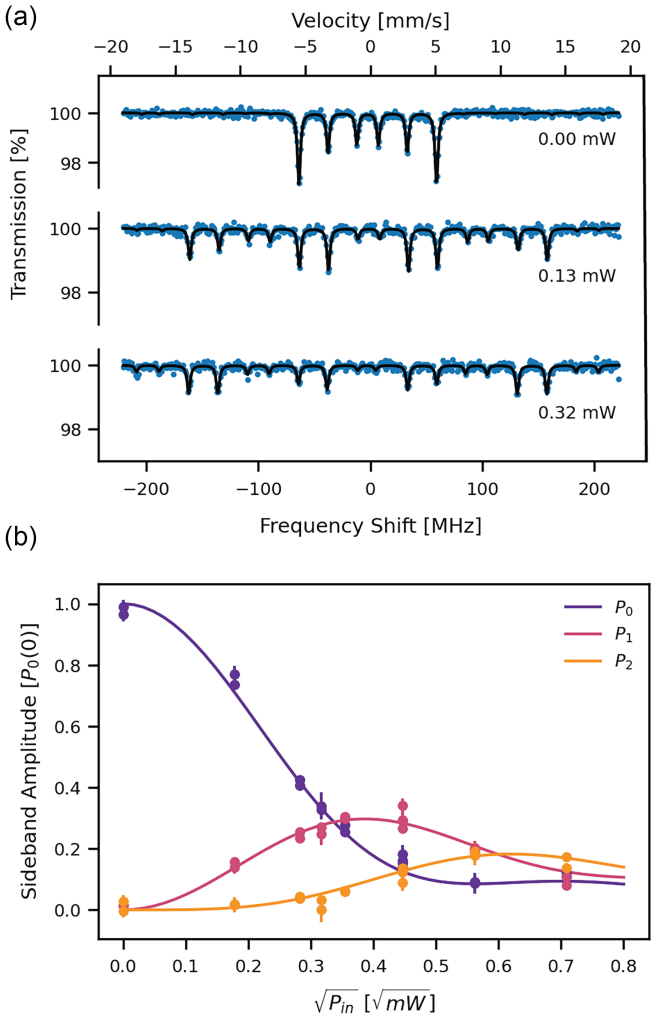

FIG. 3. (a) Mössbauer absorption spectra of the device with no SAW excitation and two cases of increasing SAW drive power. As the modulation strength grows, higher-order sidebands emerge while amplitudes decrease to maintain a constant overall integral over the absorption spectrum. Continuous lines, overlaying the data points, represent fits to the data [22]. (b) Reconstructed amplitudes of the first three sidebands accessible within the available velocity range, as a function of the applied SAW drive power. The solid lines are a global fit to all three datasets using a model based on the squared Bessel functions integrated over the SAW amplitude distribution. The two fit parameters are the modulation scaling factor $C_\perp$ and the reflection coefficient α, which encodes the degree of standing-wave formation due to SAW reflections.

to 18 visible absorption peaks, as shown in Fig. 3(a), which reduce, due to symmetry and the known hyperfine structure, to 7 distinct features with characteristic amplitudes which follow combinations of squared Bessel functions $J_n^2(m)$ up to order $n = 2$. Notably, the natural Zeeman splitting in α-Fe (24.4 MHz) happens to be one fourth of the SAW modulation frequency (97.9 MHz), resulting in spectral overlap between certain sidebands and the unshifted hyperfine lines, within our instrumental resolution. While this overlap has no consequence for our experiment, which employs an incoherent source, synchrotron-based excitation would lead to interference between the unmodulated transitions and the overlapping sidebands.

To extract quantitative information, each spectrum is fit using a sum of Lorentzian peaks overlaid on a fifth-order polynomial baseline, accounting for the change in solid angle in the scan, nonuniform channel sampling, and slow drifts in detector response. The fit yields precise absorption peak locations that allow the calibration of the Doppler velocity scale over the full ± 19 mm/s range [22]. Each spectrum is then normalized by its polynomial baseline, resulting in the spectra in Fig. 3(a), and the area under each peak is integrated. From the resulting integrated spectra, the area of each sideband can be directly evaluated. Combined with knowledge of the power delivered to the SAW coupler, this enables the reconstruction of the modulation indices $k_0 A(P_{\mathrm{in}})$. The residual reflection from the output transducer results in a spatially inhomogeneous SAW amplitude along the propagation direction which can then be expressed as $A(x) = A_0\sqrt{1+\alpha^2+2\alpha\cos(k_{\mathrm{SAW}}x)}$, where A_0 is the amplitude of the forward-propagating wave, α is the coherent reflection coefficient, and k_{SAW} is the SAW wave number. To account for this effect, the model described in Eq. (1) is integrated over the amplitude distribution, yielding a modified prediction for the sideband structure [11,22,23]. Both the out-of-plane displacement conversion constant $C_\perp = (5.35 \pm 0.37) \times 10^{-9}$ m/$\sqrt{\mathrm{W}}$ and the reflected wave fraction $\alpha = 0.36 \pm 0.02$ are extracted by fitting this extended model [Fig. 3(b)]. These values are in excellent agreement with electromechanical calculations for an ST-cut quartz substrate supporting a Rayleigh-type surface acoustic wave, based on the known elastic constants of quartz [22,24,35], and are consistent with near-unity transfer of the SAW displacement to the ^{57}Fe film within experimental uncertainty.

Discussion and outlook—The results presented here demonstrate the successful dynamic modulation of Mössbauer nuclear energy levels using 97.9 MHz surface acoustic waves. This high-frequency control, both in speed and in phase coherence, establishes a new regime of acoustic-nuclear coupling. Unlike lower-frequency or quasistatic piezodriven systems, SAWs offer the advantage of continuous, propagating phase control at gigahertz bandwidths. In addition, this is achieved in a fully monolithic device, enabling scalable fabrication with the robustness and flexibility of solid-state architectures. Looking forward, we envision several developments of this technology. First, SAW transducers can be engineered to allow nearly arbitrary mechanical drive, enabled by multiharmonic excitation [36] or by chirped designs [37]. Combined with synchrotron radiation (with x-ray spot sizes smaller than the SAW wavelength) such devices would allow fast, coherent programmable modulation of nuclear transitions, extending the reach of time-domain control protocols in

nuclear quantum optics, including fast phase-jump and interferometric schemes [12,13,38]. Beyond waveform control, the broad tunability of the SAW frequency and amplitude provides a stable and precisely controllable Doppler shift of thin Mössbauer absorbers. This capability could significantly enhance the dynamic range of Mössbauer spectrometers, enabling high-precision spectroscopy at much higher Doppler shifts. A complementary direction is to couple the nuclear resonance to a surface acoustic wave resonator operated at cryogenic temperatures [14–16,19], opening a path toward optomechanical experiments in the x-ray regime [39]. While single-phonon, single-photon strong coupling is not currently accessible with state-of-the-art SAW resonators, such devices in the quantum regime can nevertheless serve as high-fidelity, quantum-calibrated probes of the local mechanical and thermal environment governing the nuclear states of Mössbauer films. Finally, the ability to couple surface acoustic waves to nuclear transitions may offer a promising route for the dynamic control of nuclear clocks [40–42], in particular the ^{229}Th isomeric transition which was recently observed in a $^{229}ThF_4$ thin film [43], potentially enabling mechanical modulation of ultrastable, nuclear optical transitions, and establishing a new interface between solid-state mechanics and nuclear quantum metrology.

Acknowledgments—We thank Professor D. Ryan (McGill) for early advice on Mössbauer spectroscopy and Professor D. Goldhaber-Gordon (Stanford) for advice on the design and fabrication of the SAW devices. This work was supported by the U.S. Air Force Office of Scientific Research under Award No. FA9550-22-1-0439, and by the "Table-top experiments for fundamental physics" program, sponsored by the Gordon and Betty Moore Foundation, Simons Foundation, Alfred P. Sloan Foundation, and John Templeton Foundation. Sample fabrication was partially supported by the U.S. Department of Energy, Office of Science, Basic Energy Sciences, Materials Sciences and Engineering Division, under Contract No. DE-AC02-76SF00515. Part of this work was performed at the Stanford Nano Shared Facilities (SNSF) and the Stanford Nanofabrication Facility (SNF), both of which are supported by the National Science Foundation under Award No. ECCS-2026822.

Data availability—The data that support the findings of this article are not publicly available. The data are available from the authors upon reasonable request.

[1] R. L. Mössbauer, Kernresonanzabsorption von γ-Strahlung in Ir191, Z. Naturforsch. **14A**, 211 (1959).
[2] R. V. Pound and G. A. Rebka, Apparent weight of photons, Phys. Rev. Lett. **4**, 337 (1960).
[3] P. Gütlich, E. Bill, and A. X. Trautwein, *Mössbauer Spectroscopy and Transition Metal Chemistry* (Springer, Berlin, 2011), 10.1007/978-3-540-88428-6.
[4] B. W. Adams *et al.*, X-ray quantum optics, J. Mod. Opt. **60**, 2 (2013).
[5] R. Röhlsberger, H.-C. Wille, K. Schlage, and B. Sahoo, Electromagnetically induced transparency with resonant nuclei in a cavity, Nature (London) **482**, 199 (2012).
[6] J. Haber *et al.*, Collective strong coupling of x-rays and nuclei in a nuclear optical lattice, Nat. Photonics **10**, 445 (2016).
[7] D. Lentrodt, C. H. Keitel, and J. Evers, Toward nonlinear optics with Mössbauer nuclei using x-ray cavities, Phys. Rev. Lett. **135**, 033801 (2025).
[8] N. D. Heiman, L. Pfeiffer, and J. C. Walker, rf-induced sidebands in Mössbauer spectra, Phys. Rev. Lett. **21**, 93 (1968).
[9] S. L. Ruby and D. I. Bolef, Acoustically modulated γ rays from ^{57}Fe, Phys. Rev. Lett. **5**, 5 (1960).
[10] A. R. Mketchyan, G. A. Arutyunyan, A. R. Arakelyan, and R. G. Gabrielyan, Modulation of Mössbauer radiation by coherent ultrasonic excitation in crystals, Phys. Status Solidi (b) **92**, 23 (1979).
[11] H. Yamashita, S. Kitao, Y. Kobayashi, H. Ota, R. Masuda, K. Fujiwara, T. Mitsui, and M. Seto, Measurement of the sub-nanometer vibration amplitudes using ^{57}Fe synchrotron Mössbauer source, Interactions **245**, 15 (2024).
[12] F. Vagizov, V. Antonov, Y. V. Radeonychev, R. N. Shakhmuratov, and O. Kocharovskaya, Coherent control of the waveforms of recoilless γ-ray photons, Nature (London) **508**, 80 (2014).
[13] K. P. Heeg *et al.*, Spectral narrowing of x-ray pulses for precision spectroscopy with nuclear resonances, Science **357**, 375 (2017).
[14] M. J. A. Schuetz, E. M. Kessler, G. Giedke, L. M. K. Vandersypen, M. D. Lukin, and J. I. Cirac, Universal quantum transducers based on surface acoustic waves, Phys. Rev. X **5**, 031031 (2015).
[15] R. Manenti, M. J. Peterer, A. Nersisyan, E. B. Magnusson, A. Patterson, and P. J. Leek, Surface acoustic wave resonators in the quantum regime, Phys. Rev. B **93**, 041411 (2016).
[16] K. J. Satzinger *et al.*, Quantum control of surface acoustic wave phonons, Nature (London) **563**, 661 (2018).
[17] L. Sletten, B. Moores, J. Viennot, and K. Lehnert, Resolving phonon Fock states in a multimode cavity with a double-slit qubit, Phys. Rev. X **9**, 021056 (2019).
[18] D. A. Golter, T. Oo, M. Amezcua, K. A. Stewart, and H. Wang, Optomechanical quantum control of a nitrogen-vacancy center in diamond, Phys. Rev. Lett. **116**, 143602 (2016).
[19] S. D. Patel, K. Parto, M. Choquer, N. Lewis, S. Umezawa, L. Hellman, D. Polishchuk, and G. Moody, Surface acoustic wave cavity optomechanics with atomically thin *h*-BN and WSe_2 single-photon emitters, PRX Quantum **5**, 010330 (2024).
[20] M. B. Schulz, B. J. Matsinger, and M. G. Holland, Temperature dependence of surface acoustic wave velocity on α quartz, J. Appl. Phys. **41**, 2755 (1975).
[21] Iron analytics 5th gen., https://www.iron-analytics.com/.
[22] See Supplemental Material at http://link.aps.org/supplemental/10.1103/tc97-98f7 for theoretical and experimental details, which includes Refs. [11,14,22–33].

[23] T. M. Aivazyan, I. M. Aivazyan, A. R. Mkrtchyan, and L. A. Kocharyan, On the determination of parameters of Mössbauer absorption spectra at ultrasonic excitation, Phys. Status Solidi (b) **64**, 757 (1974).
[24] A. Slobodnik, Surface acoustic waves and SAW materials, Proc. IEEE **64**, 581 (1976).
[25] M. O. Scully and M. S. Zubairy, *Quantum Optics* (Cambridge University Press, Cambridge, England, 1997).
[26] V. Weisskopf and E. Wigner, Berechnung der natürlichen Linienbreite auf Grund der Diracschen Lichttheorie, Z. Phys. **63**, 54 (1930).
[27] P. A. Kuchment, Floquet theory for partial differential equations, Russ. Math. Surv. **37**, 1 (1982).
[28] M. Salkola and S. Stenholm, Time-dependent perturbation of Mössbauer spectra, Phys. Rev. A **41**, 3838 (1990).
[29] M. Aspelmeyer, T. J. Kippenberg, and F. Marquardt, Cavity optomechanics, Rev. Mod. Phys. **86**, 1391 (2014).
[30] G. Dattoli, A. Torre, and S. Lorenzutta, Theory of multivariable bessel functions and elliptic modular functions, Le Matematiche **LIII**, 387 (1998), https://lematematiche.dmi.unict.it/index.php/lematematiche/article/view/376.
[31] C. Cohen-Tannoudji, J. Dupont-Roc, and G. Grynberg, *Atom-Photon Interactions: Basic Processes and Applications* (John Wiley and Sons, New York, 1998).
[32] K. Kurokawa, Power waves and the scattering matrix, IEEE Trans. Microwave Theory Tech. **13**, 194 (1965).
[33] C. E. Violet and D. N. Pipkorn, Mössbauer line positions and hyperfine interactions in α iron, J. Appl. Phys. **42**, 4339 (1971).
[34] G. Longworth and B. Window, The preparation of narrow-line Mössbauer sources of ^{57}Co in metallic matrices, J. Phys. D **4**, 835 (1971).
[35] G. A. Coquin and H. F. Tiersten, Analysis of the excitation and detection of piezoelectric surface waves in quartz by means of surface electrodes, J. Acoust. Soc. Am. **41**, 921 (1967).
[36] A. Stejskal, V. Vrba, and V. Procházka, Toward flexible intensity control of resonantly scattered γ-rays using multi-frequency vibrating resonant absorber, Appl. Phys. Lett. **126**, 084102 (2025).
[37] D. Fall, M. Duquennoy, M. Ouaftouh, N. Smagin, B. Piwakowski, and F. Jenot, Generation of broadband surface acoustic waves using a dual temporal-spatial chirp method, J. Acoust. Soc. Am. **142**, EL108 (2017).
[38] M. Gerharz *et al.*, Dark-fringe interferometer with dynamic phase control for Mössbauer science, arXiv:2509.24658.
[39] W.-T. Liao and A. Pálffy, Optomechanically induced transparency of x-rays via optical control, Sci. Rep. **7**, 321 (2017).
[40] Y. Shvyd'ko *et al.*, Resonant x-ray excitation of the nuclear clock isomer ^{45}Sc, Nature (London) **622**, 471 (2023).
[41] J. Tiedau *et al.*, Laser excitation of the Th-229 nucleus, Phys. Rev. Lett. **132**, 182501 (2024).
[42] R. Elwell, C. Schneider, J. Jeet, J. E. S. Terhune, H. W. T. Morgan, A. N. Alexandrova, H. B. Tran Tan, A. Derevianko, and E. R. Hudson, Laser excitation of the ^{229}Th nuclear isomeric transition in a solid-state host, Phys. Rev. Lett. **133**, 013201 (2024).
[43] C. Zhang *et al.*, $^{229}ThF_4$ thin films for solid-state nuclear clocks, Nature (London) **636**, 603 (2024).